

Studying Disease Reinfection Rates, Vaccine Efficacy and the Timing of Vaccine Rollout in the context of Infectious Diseases

Elizabeth Amona¹, Indranil Sahoo¹, Edward Boone¹, Ryad Ghanam²

¹*Department of Statistical Sciences and Operations Research, Virginia Commonwealth University, Richmond, United States*

²*Department of Liberal Arts and Sciences, Virginia Commonwealth University in Qatar, Doha, Qatar*

Abstract

Qatar has undergone distinct waves of COVID-19 infections, compounded by the emergence of variants, posing additional complexities. This research uniquely delves into the varied efficacy of existing vaccines and the pivotal role of vaccination timing in the context of COVID-19. Departing from conventional modeling, we introduce two models that account for the impact of vaccines on infections, reinfections, and deaths. Recognizing the intricacy of these models, we use the Bayesian framework and specifically utilize the Metropolis-Hastings Sampler for estimation of model parameters. The study conducts scenario analyses on two models, quantifying the duration during which the healthcare system in Qatar could have potentially been overwhelmed by an influx of new COVID-19 cases surpassing the available hospital beds. Additionally, the research explores similarities in predictive probability distributions of cumulative infections, reinfections, and deaths, employing the Hellinger distance metric. Comparative analysis, employing the Bayes factor, underscores the plausibility of a model assuming a different susceptibility rate to reinfection, as opposed to assuming the same susceptibility rate for both infections and reinfections. Results highlight the adverse outcomes associated with delayed vaccination, emphasizing the efficacy of early vaccination in reducing infections, reinfections, and deaths. Our research advocates prioritizing early vaccination as a key strategy in effectively combating future pandemics. This study contributes vital insights for evidence-based public health interventions, providing clarity on vaccination strategies and reinforcing preparedness for challenges posed by infectious diseases. The data set and implementation code for this project is made available at <https://github.com/elizabethamona/VaccinationTiming>.

Keywords: Bayes factor; Compartmental models; COVID-19; Epidemiology; Hellinger distance; Kernel density estimation

1 Introduction

The relentless battle against the severe acute respiratory syndrome coronavirus 2 (SARS-CoV-2) continues to unveil new complexities in the dynamics of infectious diseases and the effectiveness of interventions. As the pandemic progresses, one aspect that has garnered significant attention is the phenomenon of reinfection — a topic both timely and imperative for further exploration. Reinfection with SARS-CoV-2 occurs when an individual contracts the virus, recovers, and subsequently becomes infected again. While most reinfections tend to be mild, severe illness can also occur (Willyard, 2023; CDC, 2023). People who are reinfected can also spread the virus to others, and staying up to date with vaccine doses and starting treatment within days after developing symptoms can decrease a person’s risk of experiencing severe illness from reinfection (CDC, 2023).

The State of Qatar, like many countries, has experienced distinct waves of COVID-19 infections. From the initial surge of cases to the subsequent introduction of new variants, Qatar’s experience serves as an insightful case study. In Qatar, an initial wave of infections occurred between March and June 2020, resulting in the development of detectable antibodies against SARS-CoV-2 in approximately 40% of the population. Subsequently, the country experienced two consecutive waves of infections from January to May 2021, triggered by the emergence of the B.1.1.7 (alpha) and B.1.351 (beta) variants (Abu-Raddad et al., 2021a). Other variants such as Omicron and its subvariants have also emerged (Chemaitelly et al., 2021). Understanding the patterns of infections, reinfections, and associated mortality in the presence of effective vaccination is crucial for guiding effective public health strategies. To this end, this research presents a comprehensive methodology to examine the impact of variations in vaccine efficacy and the timing of vaccine administration in the context of infectious diseases. The proposed methodology has been implemented to

analyze the dynamics of COVID-19 in terms of infections, reinfections, and deaths within Qatar.

Various studies have investigated the impact of vaccination effectiveness on infections and deaths globally, employing mathematical frameworks or case-control designs. Amona et al. (2023) developed a mathematical (SEIRDV) model to study the effectiveness of vaccination in the reduction of secondary cases and mortality rate in Qatar. The authors concluded that vaccines drastically reduced the basic reproduction number, R_0 and saved lives. Ghosh and Ghosh (2023) employed an SEIR model to determine the required vaccine efficiency to diminish infection and mortality peaks in Italy, India, and Australia. Results indicated substantial reductions with specific vaccine efficiency and coverage combinations; for example, a 75% efficient vaccine administered to 50% of the population can reduce the peak number of infected individuals by nearly 50% in Italy. Andrews et al. (2022) conducted a test-negative case-control study in England to estimate vaccine effectiveness against omicron and delta variants, revealing effectiveness against symptomatic disease, but highlighting waning protection over time. Some studies have further delved into the possibility of reinfection after the waning of the vaccines. Hammerman et al. (2022) performed a retrospective cohort study in Israel, revealing a sixfold higher reinfection rate among the unvaccinated compared to the vaccinated, highlighting vaccine effectiveness and waning protection. Additional cohort studies on vaccine effectiveness and reinfection risks post-waning are documented in Hiam and Abu-Raddad (2022); Lewis et al. (2022); Hall et al. (2022); Sheehan et al. (2021); Rahman et al. (2022). Notably, these studies exclusively employed cohort designs. Mukandavire et al. (2020) explored scenario analysis early in the pandemic using an SEIR model in South Africa in a different context.

Thus, after an extensive literature review, several research gaps in the context of studying the dynamics of infectious diseases have emerged. Firstly, timely vaccine availability is

identified as a significant concern that requires further investigation. Secondly, there is a notable absence of mathematical models that explicitly explain the degree of susceptibility after infection resulting from the waning of vaccination. The lack of such models leave a critical gap in understanding the dynamics of post-vaccination susceptibility. Thirdly, a gap also exists in the realm of scenario analysis on vaccine efficacy. No study has comprehensively explored how variations in vaccine efficacy might impact infection, reinfection, and mortality rates. This gap underscores the need for research that delves into the broader implications of vaccine efficacy on different aspects of disease dynamics.

The uniqueness of our study lies in its emphasis on scenario analysis of vaccine efficacy, closely reflecting the real-world dynamics of vaccination efforts. In this context, we explore the impact of these variations on the spread of the virus, as well as the occurrence of reinfections and mortality. In conjunction with vaccine efficacy, the timing (early or late) of vaccine roll out is identified as an important factor. The choice between early and late vaccine administration holds implications for achieving population-level immunity and attenuating the impact of the virus. To better reflect real-world scenarios, we propose two mathematical models with different dynamics and under different assumptions (see Section 2). This work deviates from traditional mathematical modeling by not only estimating parameters and studying system dynamics based on real data, but also projecting various scenarios relevant to infectious diseases, specifically COVID-19. Furthermore, while conventional models change parameter values to study the efficacy and impact of vaccination, we are changing when the interventions and/or vaccinations were implemented to explore the dynamics, which makes our study novel. Given our proposed models and the estimated parameter values, we seek to address the following research questions: What would have happened if vaccines were administered at different time points, either earlier or later? In scenarios with limited government interventions, what potential consequences might arise?

Is there a possibility that delaying vaccine administration could lead to a scenario where the number of infections exceeds the capacity of the country’s healthcare system, specifically in terms of available hospital beds?? We aim to calculate the number of days on which such system breakdowns might occur, should vaccines be administered late. Thus, our objective is to utilize the proposed mathematical models as a tool to answer the above research questions and understand and interpret the consequences of these different strategies, rather than just parameter estimation or data fitting.

1.1 Motivation for model comparison

In order to explain the real-world dynamics of infectious diseases, we introduce two mathematical models, each offering a different viewpoint on the complex interaction among diseases, immunity, and vaccination. The first model assumes that individuals who recover from their initial infection might exhibit different susceptibility rates upon re-exposure. This assumption reflects the idea that immunity wanes over time and that those who have recovered from the disease may still be at risk, although at a different rate before reinfection. This model thus considers different susceptibility rates among different segments of the population, and their impact on the overall course of the disease.

In contrast, the second model does not account for the varying susceptibility of those who have recovered, thereby taking a more straightforward approach and assuming a uniform susceptibility rate among all individuals. We describe the two models in Section 2, thereby exploring the question: Does the first model, with its complex assumptions about variable susceptibility, represent real-world dynamics better? Or does the simplicity of the second model give a more accurate picture? Thus, our approach gives data-driven insights into the real-world implications of varying susceptibility rates, immunity waning, and vaccination efficacy. As such, this study provides a clearer understanding of disease dynamics

in the presence of evolving immunity, and guidance for public health interventions and decision-making in a complex, ever-changing world.

2 The Compartmental Models

The models presented in this paper are an extension of the SEIRDV model as introduced by Amona et al. (2023). Hence, all assumptions inherent to the SEIRDV model remain applicable to our proposed models. In these models, t serves as a time index, denoting the number of days elapsed since the first recorded case of COVID-19 within the population of interest. At any given time t , $S(t)$ denotes the total number of susceptible individuals, $S_1(t)$ represents the number of individuals who are susceptible and have not contracted the disease, $E(t)$ denotes the number of individuals who are in the exposed state, $I(t)$ denotes the total number of individuals who are infected (displaying symptoms), $R_E(t)$ denotes the cumulative number of individuals who have recovered following exposure, $R_I(t)$ denotes the cumulative number of individuals who have recovered following infection, $D(t)$ denotes the cumulative number of deaths, $S_2(t)$ denotes the cumulative number of individuals who have regained susceptibility after their initial infection, $I_I(t)$ denotes the cumulative number of individuals who have experienced reinfection, $R_R(t)$ denotes the cumulative number of individuals who have recovered following reinfection, and $V(t)$ denotes the cumulative number of vaccinated individuals.

2.1 The $S_1EIRDVS_2I_IR_R$ Model

In addition to the inherent model assumptions, we assume that individuals who have previously been infected would develop antibodies for a certain period before these antibodies naturally wane. Subsequently, these individuals transition to a different Susceptible com-

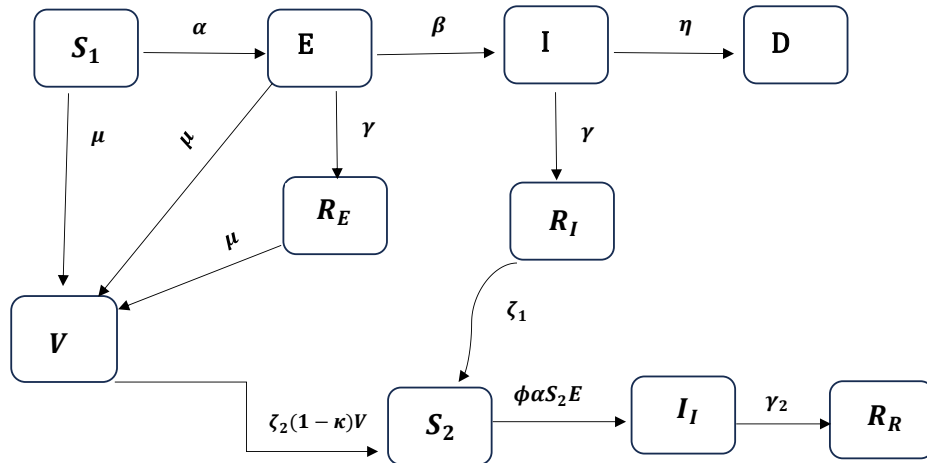


Figure 1: Schematic diagram of $S_1EIRDVS_2IIRR$ model for Covid-19

partment (S_2) at a different rate compared to the initial Susceptible compartment (S_1). Additionally, we assume that the waning of natural immunity and immunity resulting from vaccination occur at different rates, denoted as ζ_1 (representing natural immunity waning) and $\zeta_2(1 - \kappa)$ (representing vaccination-induced waning). Moreover, we assume that all individuals who experience reinfection would recover and transition to a secondary recovery compartment (R_R). We do not consider any deaths following reinfection. This assumption is supported by research indicating that the risk of severe reinfection in the State of Qatar was only approximately 1% of the risk faced by individuals who had not been previously infected (Abu-Raddad et al., 2021a). The compartmental model $S_1EIRDVS_2IIRR$ thus comprises of ten distinct compartments, and a visual representation is presented in Figure 1.

Following the flow diagram given in Figure 1 and the modeling assumptions described

above, Model 1 can be formally represented by the following system of equations:

$$\begin{aligned}
\frac{dS_1}{dt} &= -\alpha S_1(t)E(t) - \mu S_1(t), \\
\frac{dE}{dt} &= \alpha S_1(t)E(t) - (\beta + \gamma_1 + \mu)E(t), \\
\frac{dI}{dt} &= \beta E(t) - (\gamma_1 + \eta)I(t), \\
\frac{dR_E}{dt} &= \gamma_1 E(t) - \mu R_E(t), \\
\frac{dR_I}{dt} &= \gamma_1 I(t) - \zeta_1 R_I(t), \\
\frac{dD}{dt} &= \eta I(t), \\
\frac{dS_2}{dt} &= \zeta_1 R_I(t) - \phi \alpha S_2(t)E(t) + \zeta_2(1 - \kappa)V(t), \\
\frac{dI_I}{dt} &= \phi \alpha S_2(t)E(t) - \gamma_2 I_I(t), \\
\frac{dR_R}{dt} &= \gamma_2 I_I(t), \\
\frac{dV}{dt} &= \mu(S_1(t) + E(t) + R_E(t)) - \zeta_2(1 - \kappa)V(t),
\end{aligned} \tag{1}$$

with the following constraints $S_1(t) \geq 0$, $S_2(t) \geq 0$, $E(t) \geq 0$, $I(t) \geq 0$, $I_I(t) \geq 0$, $R_E(t) \geq 0$, $R_I(t) \geq 0$, $R_R(t) \geq 0$, $D(t) \geq 0$, and $V(t) \geq 0$. All parameters in system (1) are positive and are explained as follows: α is the transmission rate (per day \times individual²) from Susceptible to Exposed, β denotes the rate (per day) at which Exposed become Infected (symptomatic), γ_1 is the rate (per day) at which Infected become Recovered, ϕ is the rate (per day \times individual²) at which those who recovered from the first infections become reinfected, γ_2 is the rate (per day) at which the Reinfected become Recovered, the vaccination rate (per day) is denoted by μ , the efficacy of the vaccine is denoted by κ , where $0 < \kappa \leq 1$, the waning of the natural immunity and vaccine immunity are denoted

by ζ_1 and ζ_2 respectively, and the mortality rate (per day) for those Infected is denoted by η . Note that $\gamma_2 = 1$, which means that everyone who got reinfected recovers after a while, as a consequence of one of our assumptions.

2.2 The SEIRDV $I_I R_R$ Model

In this model, we assume that individuals who recover after the first infection could become reinfected within a short period of time if they come in contact with exposed individuals. In Model 2.2, we do not have the second susceptible compartment (S_2) as we had in Model 2.1. This means that when an individual recovers, they would automatically move into the reinfected compartment after the natural immunity wanes, as opposed to Model 2.1, which assumes that there is a delay between recovery and reinfections through the second susceptible compartment (S_2) and that the susceptibility rate differs. The remaining assumptions of this model are similar to the previous model. A visual representation is presented in Figure 2.

Following the flow diagram given in Figure 2 and the modeling assumptions described above, we represent Model 2 using the following system of equations:

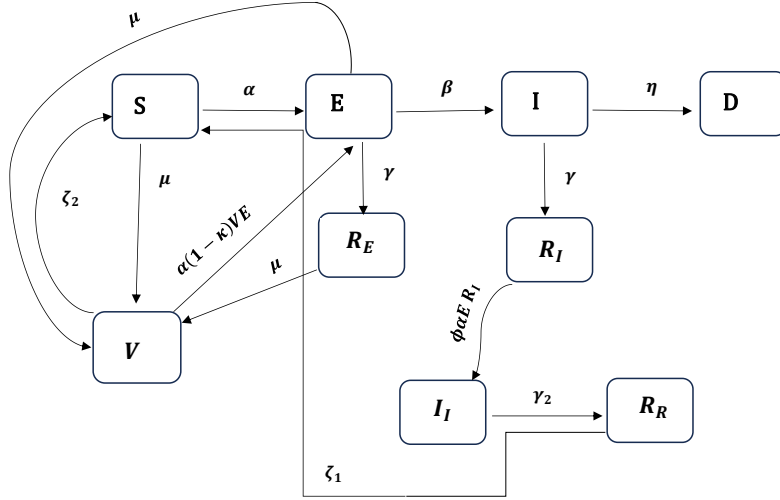


Figure 2: Schematic diagram of SEIRDV_{I_I}R_R model for Covid-19

$$\begin{aligned}
\frac{dS}{dt} &= -\alpha S(t)E(t) - \mu S(t) + \zeta_1 R_R(t) + \zeta_2 V(t), \\
\frac{dE}{dt} &= \alpha S(t)E(t) - (\beta + \gamma_1 + \mu)E(t) + \alpha(1 - \kappa)V(t)E(t), \\
\frac{dI}{dt} &= \beta E(t) - (\gamma_1 + \eta)I(t), \\
\frac{dR_E}{dt} &= \gamma_1 E(t) - \mu R_E(t), \\
\frac{dR_I}{dt} &= \gamma_1 I(t) - \alpha \phi E(t) R_I(t), \\
\frac{dD}{dt} &= \eta I(t), \\
\frac{dI_I}{dt} &= \alpha \phi E(t) R_I(t) - \gamma_2 I_I(t), \\
\frac{dR_R}{dt} &= \gamma_2 I_I(t) - \zeta_1 R_R(t), \\
\frac{dV}{dt} &= \mu(S(t) + E(t) + R_E(t)) - \zeta_2 V(t) - \alpha(1 - \kappa)V(t)E(t),
\end{aligned} \tag{2}$$

with the following constraints $S(t) \geq 0$, $E(t) \geq 0$, $I(t) \geq 0$, $I_I(t) \geq 0$, $R_E(t) \geq 0$, $R_I(t) \geq 0$, $R_R(t) \geq 0$, $D(t) \geq 0$, and $V(t) \geq 0$. All model parameters can be interpreted similarly as those discussed in subsection 2.1.

3 Statistical Methodology for Model Inference and Model Comparison

3.1 The Bayesian Analysis Framework

Given the evolving nature of the pandemic and the interventions by governments to influence various parameters, assuming a “steady state” for the dynamic system is inappropriate. Hence, we allow the transmission, recovery and reinfection rates in our models to vary over time. We define the transmission rate vector as $\boldsymbol{\alpha} = (\alpha_0, \alpha_1, \dots, \alpha_m)^T$, where $\alpha(t) = \alpha_{m-1}$ if $t_{m-1} \leq t < t_m$. Since $\alpha(t) > 0$ for all t , we have $\alpha_i > 0, i = 0, 1, \dots, m$. Similarly, we define the recovery rate vector as $\boldsymbol{\gamma}_1 = (\gamma_{10}, \gamma_{11}, \dots, \gamma_{1l})^T, l \leq m$, where each of the γ 's are independent and denotes the changed recovery rate once an intervention has been administered. We write $\gamma_1(t) = \gamma_{1l-1}$, if $t'_{l-1} \leq t < t'_l$, where $t'_1, t'_2, \dots, t'_l \in \{t_1, t_1 + 1, t_1 + 2, \dots, t_2, t_2 + 1, \dots, t_m\}$. Since $\gamma_1(t) > 0$ for all t , we have $\gamma_{1j} > 0, j = 0, 1, \dots, l$. Similarly, the reinfection rate vector is written as $\boldsymbol{\phi} = (\phi_0, \phi_1, \dots, \phi_p)^T$, where $\phi(t) = \phi_{p-1}$ if $t''_{p-1} \leq t < t''_p$ with $\phi_k > 0, k = 0, 1, \dots, p$ and $t''_1, t''_2, \dots, t''_p \in \{t_1, t_1 + 1, t_1 + 2, \dots, t_2, t_2 + 1, \dots, t_m\}$.

Thus, for $i = 0, 1, \dots, m, j = 0, 1, \dots, l$ and $k = 0, 1, \dots, p$, the system of equation in 1 becomes

$$\begin{aligned}
\frac{d\lambda_{S_1}}{dt} &= -\alpha_i \lambda_{S_1}(t) \lambda_E(t) - \mu \lambda_{S_1}(t), \\
\frac{d\lambda_E}{dt} &= \alpha_i \lambda_{S_1}(t) \lambda_E(t) - (\beta + \gamma_{1j} + \mu) \lambda_E(t), \\
\frac{d\lambda_I}{dt} &= \beta \lambda_E(t) - (\gamma_{1j} + \eta) \lambda_I(t), \\
\frac{d\lambda_{R_E}}{dt} &= \gamma_{1j} \lambda_E(t) - \mu \lambda_{R_E}(t), \\
\frac{d\lambda_{R_I}}{dt} &= \gamma_{1j} \lambda_I(t) - \zeta_1 \lambda_{R_I}(t), \\
\frac{d\lambda_D}{dt} &= \eta \lambda_I(t), \\
\frac{d\lambda_{S_2}}{dt} &= \zeta_1 \lambda_{R_I}(t) - \phi_k \alpha_i \lambda_{S_2}(t) \lambda_E(t) + \zeta_2 (1 - \kappa) \lambda_V(t), \\
\frac{d\lambda_{I_I}}{dt} &= \phi_k \alpha_i \lambda_{S_2}(t) \lambda_E(t) - \gamma_2 \lambda_{I_I}(t), \\
\frac{d\lambda_{R_R}}{dt} &= \gamma_2 \lambda_{I_I}(t), \\
\frac{d\lambda_V}{dt} &= \mu (\lambda_{S_1}(t) + \lambda_E(t) + \lambda_{R_E}(t)) - \zeta_2 (1 - \kappa) \lambda_V(t),
\end{aligned} \tag{3}$$

Similarly, the system of equation in 2 becomes

$$\begin{aligned}
\frac{d\lambda_{S_1}}{dt} &= -\alpha_i \lambda_{S_1}(t) \lambda_E(t) - \mu \lambda_{S_1}(t) + \zeta_1 \lambda_{R_R}(t) + \zeta_2 \lambda_V(t), \\
\frac{d\lambda_E}{dt} &= \alpha_i \lambda_{S_1}(t) \lambda_E(t) - (\beta + \gamma_{1j} + \mu) \lambda_E(t) + \alpha_i (1 - \kappa) \lambda_V(t) \lambda_E(t), \\
\frac{d\lambda_I}{dt} &= \beta \lambda_E(t) - (\gamma_{1j} + \eta) \lambda_I(t), \\
\frac{d\lambda_{R_E}}{dt} &= \gamma_{1j} \lambda_E(t) - \mu \lambda_{R_E}(t), \\
\frac{d\lambda_{R_I}}{dt} &= \gamma_{1j} \lambda_I(t) - \alpha_i \phi_k \lambda_E(t) \lambda_{R_I}(t), \\
\frac{d\lambda_D}{dt} &= \eta \lambda_I(t), \\
\frac{d\lambda_{I_I}}{dt} &= \alpha_i \phi_k \lambda_E(t) \lambda_{R_I}(t) - \gamma_2 \lambda_{I_I}(t), \\
\frac{d\lambda_{R_R}}{dt} &= \gamma_2 \lambda_{I_I}(t) - \zeta_1 \lambda_{R_R}(t), \\
\frac{d\lambda_V}{dt} &= \mu (\lambda_S(t) + \lambda_E(t) + \lambda_{R_E}(t)) - \zeta_2 \lambda_V(t) - \alpha_i (1 - \kappa) \lambda_V(t) \lambda_E(t),
\end{aligned} \tag{4}$$

where $\lambda_{S_1}(t)$, $\lambda_E(t)$, $\lambda_I(t)$, $\lambda_{R_E}(t)$, λ_{R_I} , $\lambda_{S_2}(t)$, $\lambda_V(t)$, $\lambda_{I_I}(t)$, $\lambda_{R_R}(t)$ and $\lambda_D(t)$ denote the mean parameters, respectively. The prior distributions of parameters in models 3 and 4 are chosen

as

$$\begin{aligned}
\alpha_i &\sim \text{Exp}(1), \quad i = 0, 1, \dots, m = 10, \\
\beta &\sim \text{Exp}(1), \\
\gamma_{1j} &\sim \text{Exp}(1), \quad j = 0, 1, \dots, l = 3, \\
\zeta_1 &\sim \text{Exp}(1), \\
\zeta_2 &\sim \text{Exp}(1), \\
\mu &\sim \text{Exp}(1), \\
\phi_k &\sim \text{Exp}(1), \quad k = 0, 1, \dots, p = 3, \\
\gamma_2 &\sim \text{Exp}(1), \\
\eta &\sim \text{Exp}(1), \\
\kappa &\sim \text{Be}(1, 1),
\end{aligned} \tag{5}$$

The likelihoods for $I(t)$, $R_I(t)$, $I_I(t)$, $R_R(t)$, $D(t)$ and $V(t)$ in models 3 and 4 are given by

$$\begin{aligned}
I(t) &\sim \text{Poisson}(\lambda_I(t)), \\
R_I(t) &\sim \text{Poisson}(\lambda_{R_I}(t)), \\
D(t) &\sim \text{Poisson}(\lambda_D(t)), \\
I_I(t) &\sim \text{Poisson}(\lambda_{I_I}(t)), \\
R_R(t) &\sim \text{Poisson}(\lambda_{R_R}(t)), \\
V(t) &\sim \text{Poisson}(\lambda_V(t)).
\end{aligned} \tag{6}$$

Note that $S_1(t)$, $S_2(t)$, and $E(t)$ in model 3 and $S(t)$, $E(t)$ in model 4 are not in the likelihood as they are latent states in that they are not directly observed. While the true likelihood for $\{S_1(t), S_2(t), E(t), I(t), R_E(t), R_I(t), I_I(t), R_R(t), V(t), D(t)\}$ should be multinomial, with three latent states in 3 and two latent states in 4, one of which is the largest state, the multinomial approach is challenging to apply. Hence, this work adopts

Poisson likelihood as an approximation. The posterior distribution for both models can be calculated based on the prior and likelihood specifications mentioned above. Since it is difficult to solve the posterior distribution analytically, we employ the Markov chain Monte Carlo (MCMC) technique to sample from the posterior distribution (Gelman et al., 1995). Specifically, we utilized the Metropolis-Hastings sampler (Gilks et al., 1995; Albert, 2009; Amona et al., 2023).

To tune the sampler, a series of short chains were generated and analyzed for convergence and adequate acceptance rates. These initial short chains were discarded as “burn-in” samples. The tuned sampler was used to generate 50,000 samples from the posterior distribution and trace plots were visually examined to ensure convergence (not included). All inferences, including parameter estimation and uncertainty quantification, were made from these 50,000 posterior draws. The model and sampling algorithm were custom programmed in the R statistical programming language version 3.6.3. The computations take approximately 10,800 seconds using an AMD A10-9700 3.50GHz processor with 16GB of RAM to obtain 50,000 draws from the posterior distribution. For more details on statistical inference see Wackerly et al. (2014); Casella and Berger (2021); Berger (1985).

3.2 Bayesian Model Comparison Using Bayes Factor

In Bayesian statistics, model comparison is a fundamental task that allows researchers to evaluate the relative support for different hypotheses or models using available data. Particularly, in Bayesian model comparison, the Bayes Factor (BF) is a robust and versatile tool that helps researchers evaluate the relative probability of different models. By considering both parameter uncertainty and prior information, it offers a comprehensive and principled approach to model selection. When working with posterior samples obtained through methods like the Metropolis-Hastings sampler, Bayes Factor can be especially valuable for

assessing the probability of competing models and informing decision-making in a wide range of scientific disciplines.

Furthermore, the Bayes Factor quantifies the support for one statistical model (Model 1) over another (Model 2) given the observed data. That is, the Bayes Factor offers a formal framework to test the following hypothesis based on the principles of Bayesian probability theory Jeffreys (1998).

Null Hypothesis(H_0) : Model 1 is more probable than Model 2.

Alternative Hypothesis(H_A) : Model 2 is more probable than Model 1.

The Bayes Factor is computed as the ratio of the marginal likelihoods of the two models:

$$BF_{12} = \frac{P(Data|Model\ 1)}{P(Data|Model\ 2)},$$

where, $P(Data|Model\ 1)$ is the marginal likelihood of Model 1 and $P(Data|Model\ 2)$ is the marginal likelihood of Model 2. If the Bayes Factor is greater than 1, it indicates that Model 1 is favored over Model 2. The magnitude of BF_{12} provides a measure of the strength of this preference. Larger BF_{12} values indicate stronger evidence in favor of Model 1. Conversely, Bayes Factor less than 1 suggests that Model 2 is favored over Model 1. A Bayes Factor close to 1 suggests that both models are equally plausible based on the data, thereby providing no strong evidence in favor of one model over the other Lesaffre and Lawson (2012); Kass and Raftery (1995). In our work, we compare the two models using Bayes Factor to provide a data-driven assessment of which model better represents the dynamics of the pandemic in the State of Qatar over our study period of February 28, 2020 - August 29, 2021.

3.3 Assessing ‘Closeness’ of Density Plots using Hellinger Distance

Density plots are powerful tools for visualizing and comparing probability distributions, particularly in the context of Bayesian analysis. While visual inspection of density plots can offer initial insights, quantifying the degree of ‘closeness’ between two density plots is often necessary for rigorous statistical analysis. Among several metrics such as Kullback-Leibler Divergence, Jensen-Shannon Divergence and many more, the Hellinger distance is a valuable tool for assessing the similarity or dissimilarity of density plots and enhancing the interpretability of Bayesian posterior distributions. This metric is useful for quantifying the separation or overlap between probability density functions, among other characteristics, and it offers a robust and objective approach to comparing and evaluating the results of Bayesian analyses. While Kullback-Leibler divergence is usually a more popular choice, it is not symmetric (Goutis and Robert, 1998) and hence is not suitable for our purposes. The Hellinger distance is defined as

$$H^2(f, g) = \frac{1}{2} \int \left(\sqrt{f(x)} - \sqrt{g(x)} \right)^2 dx = 1 - \int \sqrt{f(x)g(x)} dx, \quad 0 \leq H^2(f, g) \leq 1.$$

where, $f(x)$ and $g(x)$ are the two probability density functions being compared. The integral is computed over the entire support of the distributions Goldenberg and Webb (2019); Birgé (1986). The Hellinger distance produces a value between 0 and 1, where $H^2 = 0$ indicates that the two density plots are identical, $0 < H^2 < 1$ implies that the density plots share some degree of similarity, and $H^2 = 1$ suggests that the density plots are completely dissimilar with no overlap (Boone et al., 2014).

In our case, $f(x)$ and $g(x)$ are the cumulative posterior predictive distributions, estimated using kernel density smoothing (KDE) with a Gaussian kernel and default bandwidth as suggested by Scott (2015). The smoothing is implemented using the R function

`density()` from the `stats` package. Since KDEs can extend beyond the original data range, while comparing two KDEs, we ensure they (i) cover a common range of values and (ii) discretize that range identically, using an equally-spaced set of points in the analysis. The implementation details can be found in the 'ScenarioHellingerDistAnalysis.R' script at <https://github.com/elizabethamona/VaccinationTiming>. Since we focus only on infected, reinfected, and deaths in our scenario analysis (see 4.1), we smooth out the cumulative posterior predictive densities for these three states for all six scenarios using the Gaussian kernel density.

4 Results

In this section, we determine which of the two mathematical models introduced earlier more accurately reflects real-world dynamics of the COVID-19 pandemic. Specifically, we investigate the validity of the assumption that individuals recovering from initial infections transition to a second susceptible compartment at a different rate than those in the initial susceptible compartment. This assumption is explored to shed light on the complexities of understanding the impact of vaccination in the context of partial interventions. Notably, the second model omits consideration of the possibility that recovered individuals might be susceptible to reinfection at a different rate.

The initial conditions used for our analysis are presented in Table 1. We also provide the results from fitting the two models, including estimated mean parameter, 2.5% and 95% quantiles, and pseudo- R^2 of the fitted models (shown in Table 2) Boone et al. (2023); Amona et al. (2023). The results were obtained by using the 50,000 samples generated from the posterior distribution. Model fits, along with estimated credible regions, are illustrated in Figures 3 and 4, where actual data points are represented with dotted lines,

and fitted values are denoted by solid lines. These models fit quite well, as is evident from the Psuedo- R^2 values in Table 2. The rest of this section is organized as follows: Subsection 4.1 examines vaccination timing, hospital overload, and various scenario analyses of the two models. Subsection 4.2 delves into the similarity between the fitted density plots in the scenario analyses using Hellinger distance. The final subsection compares the plausibility of models 1 and 2 using the Bayes factor based on data from the State of Qatar.

Compartment	Initial conditions	Source
$S(0) = S_1(0)$	2,695,122	Population of Qatar as of December 30, 2022
$S_2(0)$	2695122/6	assumed
$V(0)$	0	From the data
$E(0)$	5	From Amona et al. (2023)
$I(0)$	1	From the data
$R_E(0) = R_I(0)$	0	From the data
$I_I(0)$	0	From the data
$R_R(0)$	0	From the data
$D(0)$	0	From the data

Table 1: Initial conditions for models 1 and 2

4.1 Scenario Analyses of Vaccine Efficacy and Timing in Hospital Overload using Models 1 and 2

At the onset of the COVID-19 pandemic, the Qatari government implemented various interventions to mitigate its spread. Among these measures, the stringent interventions

proved notably effective in curtailing the rise of new COVID-19 cases, while the more lenient interventions appeared less effective (Amona et al., 2023). Here we perform scenario analyses to assess the potential impact of not deploying the remaining stringent interventions during the COVID-19 pandemic in terms of number of days when new COVID-19 cases would surpass the total hospital bed capacity of 3134 beds for COVID-19 patients in Qatar, thereby completely overwhelming the medical system. We also aim to analyze any variations in this outcome across six potential scenarios. The vaccine was made available on day 380 (December 31, 2020), according to the available data, with an efficacy of 95% (Abu-Raddad et al., 2021b). However, the vaccine efficacy decreased as different variants emerged, leading us to choose the vaccine efficacy to be 94% in our analysis. Early vaccination is chosen to be on day 200. This is because we wanted to see the effect of the vaccine after the first wave recorded in the data (See red dotted lines in Figures 3(a) and 4(a)). Also, we chose the late vaccination to be on day 450, after the second wave in the data. Thus, the scenarios studied in this analysis are namely; 94% vaccine efficacy (scenario 1), 100% vaccine efficacy (scenario 2), early vaccine (day 200) with 94% vaccine efficacy (scenario 3), late vaccine (day 450) with 94% vaccine efficacy (scenario 4), early vaccine with 100% vaccine efficacy (scenario 5) and late vaccine with 100% vaccine efficacy (scenario 6). In each scenario, we calculate the posterior predictive distribution of the daily count of infected individuals, subsequently determining the range of number of days for which the number of infected surpasses the predefined threshold of total available beds, based on 50,000 posterior samples.

Findings from Model 1 revealed that under partial interventions, when vaccine efficacy was 94% (scenario 1), the number of days during which hospitals would have been overwhelmed ranged from 54 - 481 days. This signifies a period wherein the healthcare system would have exceeded its capacity, receiving more new patients than the established thresh-

old, lasting between 54 and 481 days. A 100% vaccine efficacy (scenario 2) would have narrowed the range down to 54 - 444 days. This underscores the significant reduction in overwhelmed days with a fully efficacious vaccine, even in the presence of partial interventions. Notably, introducing vaccines earlier (scenarios 3 and 5) did not substantially alter the overwhelmed period, which still remained at 54 - 444 days. However, if the vaccine introduction was delayed, the range considerably widened to 57 - 487 days. In summary, the analysis under Model 1 suggested that, under partial interventions, the Qatari government's provided hospital beds would never have sufficed without reaching critical capacity. Moreover, a 100% efficacious vaccine or early administration, irrespective of efficacy, would have resulted in fewer overwhelmed days compared to delayed vaccine administration.

Similar to the findings in Model 1, Model 2's analysis also revealed that under the vaccine efficacy of 94% (scenario 1), the hospitals' overwhelmed period ranged from 55 - 453 days, while a 100% efficacy (scenario 2) narrowed it to 53 - 443 days, emphasizing the significance of highly efficacious vaccines in mitigating bed capacity challenges during partial interventions. The impact of early vaccine introduction under partial interventions was consistent across efficacy rates, maintaining a relatively stable overwhelmed period of 53 - 445 days under scenario 3 and 55 - 444 days under scenario 5. However, late vaccine introduction substantially extended the potential duration of hospital overload, with scenario 4 (94% efficacy) ranging from 55 - 505 days and scenario 6 (100% efficacy) from 53 - 513 days, surprisingly showing scenario 6 to be slightly less effective than scenario 4. This discrepancy raises questions about the model's realism and underscores the need for further exploration to identify an accurate model for capturing the real world dynamics of the pandemic.

4.2 Hellinger Distance Analysis

Under each scenario, we also computed the posterior predictive distributions for cumulative infections, reinfections, and deaths at day 540, which is 10 days before the conclusion of our study period on day 550. These distributions were smoothed using kernel density smoothing (KDE) with a Gaussian kernel and default bandwidth, and then graphed. This approach allowed us to clearly visualize the impact of varying vaccine efficacies and the timing of their availability on infections, reinfections, and deaths since the onset of the pandemic and the introduction of vaccines in Qatar. Figure 5 displays the smoothed posterior predictive distributions for cumulative infections, reinfections, and deaths at day 540 from Model 1, while Figure 6 illustrates the same for Model 2. Subsequently, we conducted Hellinger distance analysis on these smoothed densities to estimate the 'closeness' of the different scenarios.

In our examination of Model 1 posterior predictive distributions of cumulative infections at day 540 out of 550 in Figure 5(a), scenarios involving the 94% efficacious vaccine (scenario 1) and the 100% efficacious vaccine (scenario 2) exhibited remarkably high similarity, indicated by a low Hellinger Distance of 0.000020, indicating that the pursuit of an ideal vaccine may not have significantly influenced the effective control of cases within the system. Conversely, dissimilarity was substantial when comparing scenarios 1 and 3 (early vaccine with 94% efficacy), with a Hellinger distance of 0.340625. Late vaccinations (scenarios 4 and 6) resulted in higher cumulative infections and demonstrated considerable dissimilarity, marked by a Hellinger distance of 0.034114, with 100% efficacy being more effective than 94% efficacy.

Shifting to reinfections posterior predictive density plots from Model 1 in Figure 5(b), scenarios 1 and 2 showed significant similarity (Hellinger Distance: 0.000179), while dissimilarity was pronounced between scenarios 1 and 3 (Hellinger Distance: 0.375517). Scenarios

3 and 5 displayed substantial similarity (Hellinger Distance: 0.000012) but scenarios 4 and 6 showed some dissimilarity (Hellinger Distance: 0.033001). Also, cumulative reinfections were likely to be around 35 on day 540 when the vaccine was administered late (scenarios 4 and 6). The most substantial dissimilarity emerged when comparing Scenarios 5 and 6, signified by a Hellinger Distance of 0.531083.

The Model 1 posterior predictive cumulative death density plots in Figure 5(c) revealed that early vaccination (scenarios 3 and 5) would have resulted in lower number of cumulative deaths compared to the observed outcomes (scenarios 1 and 2). Late vaccination (scenarios 4 and 6) would have produced a much higher cumulative death toll and vaccine efficacy mattered in this case. Significant similarity was seen between scenarios 1 and 2 (Hellinger Distance: 0.000091) and scenarios 3 and 5 (Hellinger Distance: 0.000278), while moderate to substantial dissimilarities were observed between scenarios 4 and 6 (Hellinger Distance: 0.031157) and scenarios 5 and 6 (Hellinger Distance: 0.644322) respectively. These findings show that lower infections lead to fewer deaths, while higher infections lead to higher number of deaths, thereby mimicking real-world dynamics.

In line with our analysis for Model 1, we computed Hellinger distances for the posterior predictive infected density plots in Model 2, as displayed in Figure 6(a). Unlike Model 1, scenario 1 (94% efficacious vaccine) and scenario 2 (100% efficacious vaccine) demonstrated remarkable dissimilarity (Hellinger Distance: 0.500488). Comparison between scenario 1 with scenario 3 (early vaccine with 94% efficacy) revealed a moderate degree of dissimilarity (Hellinger Distance: 0.242202), and that between scenario 3 and scenario 5 (early vaccine at 100% efficacy) displayed moderate similarity as well (Hellinger Distance: 0.013369). Conversely, the comparison between scenario 4 (late vaccine at 94% efficacy) and scenario 6 (late vaccine at 100% efficacy) revealed the most significant dissimilarity (Hellinger Distance: 0.616759). The same trend was also observed between scenarios 5 and 6 (Hellinger

Distance: 0.558894). Overall, the efficacy of the vaccine appeared to be crucial in Model 2, with a clear preference for a 100% efficacious vaccine over a 94% efficacious one, irrespective of timing of roll out.

Transitioning to reinfections posterior probability density plots in Figure 6(b), scenarios 1 and 2 exhibited substantial dissimilarity (Hellinger Distance: 0.298233). Similarly, comparing scenarios 1 and 3, we observed substantial dissimilarity (Hellinger Distance: 0.102579). Conversely, scenario 3 and scenario 5 displayed a lesser degree of dissimilarity (Hellinger Distance: 0.07729328). Additionally, scenarios 4 and 6 were found to have significant dissimilarity (Hellinger Distance: 0.5072856), while scenarios 5 and 6 were moderately dissimilar (Hellinger Distance: 0.3656723). Thus early vaccination was still preferred, as the probability of excessively high reinfections became improbable in these scenarios.

For the cumulative posterior predictive distributions of death in Figure 6(c), our analysis indicated moderate similarity between scenarios 1 and 2 (Hellinger distance: 0.094946). Considerable similarity was also observed between scenario 3 and 5 (Hellinger distance: 0.006788) and scenarios 4 and 6 (Hellinger distance: 0.001163). The most significant dissimilarity was observed when comparing scenarios 5 and 6 (Hellinger Distance: 0.440002). These results once again advocated for early vaccination, with the higher efficacious vaccine resulting in lower cumulative deaths.

4.3 Model Comparison using Bayes factor

In our study, we have introduced two distinct models, each incorporating unique underlying dynamics, aiming to identify the model better suited to explain the observed data. Model 1 introduces a secondary compartment (S_2) to account for individuals with recovered natural immunity. Additionally, it considers the waning of vaccine-induced immunity, while individuals transition to the secondary susceptible compartment at varied rates. Con-

versely, Model 2 posits that a second susceptible compartment is unnecessary. Our focus is on comparing the performance of these models through the Bayes factor metric, detailed in Subsection 3.2, to determine their relative likelihood of explaining the observed data. Based on the data, the Bayes factor ($BF_{1,2}$) was calculated to be 50013.35, which is greater than 1. Hence we conclude that Model 1 is more probable (a better fit for the data) than Model 2. This is also corroborated by the higher Pseudo- R^2 value of Model 1 compared to Model 2. Thus, the Bayes factor analysis reveals that Model 1, incorporating a secondary compartment (S_2) to accommodate individuals with recovered natural immunity and addressing the waning of vaccine-induced immunity with varied transition rates to the secondary susceptible compartment, is deemed more appropriate for representing the dynamics of the COVID-19 pandemic in the State of Qatar.

5 Discussion

In the realm of mathematical modeling, we are often tasked with studying the intricate dynamics of real-world phenomena. To this end, we implement models which offer distinct perspectives on complex systems. In this study, we introduce two such models, each providing a unique lens through which we explore an important question: How do vaccination, reinfection, and partial interventions impact the course of infectious diseases? We delve into these models with a clear goal: to understand which one aligns most closely with real-world observations. Additionally, we explore how changes in vaccine effectiveness and time of vaccine deployment impact the patterns of infections, reinfections, and deaths in these models. We also carefully examine the accuracy of certain assumptions in our models, especially the idea that people recovering from initial infections may have varying susceptibilities to reinfection.

To address these fundamental questions, we undertake a comparative analysis of our mathematical models by performing model selection using Bayes factor. Our analysis shows that based on real-life COVID-19 data from the State of Qatar, the model assuming varying susceptibilities among individuals recovering from their initial infections (Model 1) is significantly more probable than the simpler model, which assumes uniform susceptibility among all individuals (Model 2). Moreover, our approach of employing Bayes factor for model selection in the context of disease modeling is novel and, to the best of our knowledge, has not been explored before in literature.

Our research can also serve as a valuable tool for decision-makers grappling with the formulation of challenging public health policies during a pandemic. It is evident from Figure 5 (a-c) that, regardless of the vaccine's effectiveness, getting vaccinated late is not recommended. This late vaccination increases the chances of more people getting infected, reinfected, and more deaths. The timing of vaccine roll out also matters; our results show that introducing it earlier saved lives and reduced infections, although the overall decrease wasn't as significant as with early vaccination. Therefore, in the presence of partial interventions, early vaccination (scenarios 3 and 5) would be the most effective strategy in reducing active infections, reinfections, and deaths. If the vaccine had been given earlier, we could have saved more than the 50 lives, as mentioned in the study by Amona et al. (2023), and the number of infectious individuals would have decreased significantly compared to the reduction observed when the vaccine was introduced much later. As a result, our research advocates for the implementation of early vaccination protocols in the event of a future pandemic.

Acknowledgements

The authors would like to thank Virginia Commonwealth University in Qatar and Qatar Foundation for supporting this work through the VCU Qatar Mathematical Data Sciences Lab.

References

- Abu-Raddad, L. J., Chemaitelly, H., and Bertollini, R. (2021a). Severity of sars-cov-2 reinfections as compared with primary infections. *New England Journal of Medicine*, 385(26):2487–2489.
- Abu-Raddad, L. J., Chemaitelly, H., and Butt, A. A. (2021b). Effectiveness of the bnt162b2 covid-19 vaccine against the b. 1.1. 7 and b. 1.351 variants. *New England Journal of Medicine*, 385(2):187–189.
- Albert, J. (2009). An introduction to R. In *Bayesian Computation with R*, pages 1–17. Springer.
- Amona, E. B., Ghanam, R. A., Boone, E. L., Sahoo, I., and Abu-Raddad, L. J. (2023). Incorporating interventions to an extended seird model with vaccination: Application to covid-19 in qatar. *Journal of Data Science*, pages 1–19.
- Andrews, N., Stowe, J., Kirsebom, F., Toffa, S., Rickeard, T., Gallagher, E., Gower, C., Kall, M., Groves, N., O’Connell, A.-M., et al. (2022). Covid-19 vaccine effectiveness against the omicron (b. 1.1. 529) variant. *New England Journal of Medicine*, 386(16):1532–1546.

- Berger, J. O. (1985). Prior information and subjective probability. In *Statistical Decision Theory and Bayesian Analysis*, pages 74–117. Springer.
- Birgé, L. (1986). On estimating a density using hellinger distance and some other strange facts. *Probability theory and related fields*, 71(2):271–291.
- Boone, E. L., Abdel-Salam, A.-S. G., Sahoo, I., Ghanam, R., Chen, X., and Hanif, A. (2023). Monitoring seird model parameters using mewma for the covid-19 pandemic with application to the state of qatar. *Journal of Applied Statistics*, 50(2):231–246.
- Boone, E. L., Merrick, J. R., and Krachey, M. J. (2014). A hellinger distance approach to mcmc diagnostics. *Journal of Statistical Computation and Simulation*, 84(4):833–849.
- Casella, G. and Berger, R. L. (2021). *Statistical Inference*. Cengage Learning.
- CDC (2023). What is covid-19 reinfection? <https://www.cdc.gov/coronavirus/2019-ncov/your-health/reinfection.html>.
- Chemaitelly, H., Tang, P., Hasan, M. R., AlMukdad, S., Yassine, H. M., Benslimane, F. M., Al Khatib, H. A., Coyle, P., Ayoub, H. H., Al Kanaani, Z., et al. (2021). Waning of bnt162b2 vaccine protection against sars-cov-2 infection in qatar. *New England Journal of Medicine*, 385(24):e83.
- Gelman, A., Carlin, J. B., Stern, H. S., and Rubin, D. B. (1995). *Bayesian data analysis*. Chapman and Hall/CRC.
- Ghosh, S. K. and Ghosh, S. (2023). A mathematical model for covid-19 considering waning immunity, vaccination and control measures. *Scientific Reports*, 13(1):3610.

- Gilks, W. R., Richardson, S., and Spiegelhalter, D. (1995). *Markov Chain Monte Carlo in Practice*. CRC press.
- Goldenberg, I. and Webb, G. I. (2019). Survey of distance measures for quantifying concept drift and shift in numeric data. *Knowledge and Information Systems*, 60(2):591–615.
- Goutis, C. and Robert, C. P. (1998). Model choice in generalised linear models: A bayesian approach via kullback-leibler projections. *Biometrika*, 85(1):29–37.
- Hall, V., Foulkes, S., Insalata, F., Kirwan, P., Saei, A., Atti, A., Wellington, E., Khawam, J., Munro, K., Cole, M., et al. (2022). Protection against sars-cov-2 after covid-19 vaccination and previous infection. *New England Journal of Medicine*, 386(13):1207–1220.
- Hammerman, A., Sergienko, R., Friger, M., Beckenstein, T., Peretz, A., Netzer, D., Yaron, S., and Arbel, R. (2022). Effectiveness of the bnt162b2 vaccine after recovery from covid-19. *New England Journal of Medicine*, 386(13):1221–1229.
- Hiam, C. and Abu-Raddad, L. J. (2022). Waning effectiveness of covid-19 vaccines.
- Jeffreys, H. (1998). *The theory of probability*. OuP Oxford.
- Kass, R. E. and Raftery, A. E. (1995). Bayes factors. *Journal of the american statistical association*, 90(430):773–795.
- Lesaffre, E. and Lawson, A. B. (2012). *Bayesian biostatistics*. John Wiley & Sons.
- Lewis, N., Chambers, L. C., Chu, H. T., Fortnam, T., De Vito, R., Gargano, L. M., Chan, P. A., McDonald, J., and Hogan, J. W. (2022). Effectiveness associated with vaccination

after covid-19 recovery in preventing reinfection. *JAMA network open*, 5(7):e2223917–e2223917.

Mukandavire, Z., Nyabadza, F., Malunguza, N. J., Cuadros, D. F., Shiri, T., and Musuka, G. (2020). Quantifying early covid-19 outbreak transmission in south africa and exploring vaccine efficacy scenarios. *PloS one*, 15(7):e0236003.

Rahman, S., Rahman, M. M., Miah, M., Begum, M. N., Sarmin, M., Mahfuz, M., Hossain, M. E., Rahman, M. Z., Chisti, M. J., Ahmed, T., et al. (2022). Covid-19 reinfections among naturally infected and vaccinated individuals. *Scientific reports*, 12(1):1438.

Scott, D. W. (2015). *Multivariate density estimation: theory, practice, and visualization*. John Wiley & Sons.

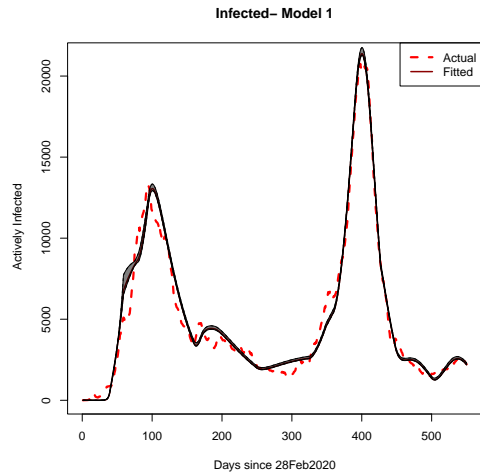
Sheehan, M. M., Reddy, A. J., and Rothberg, M. B. (2021). Reinfection rates among patients who previously tested positive for coronavirus disease 2019: a retrospective cohort study. *Clinical Infectious Diseases*, 73(10):1882–1886.

Wackerly, D., Mendenhall, W., and Scheaffer, R. L. (2014). *Mathematical Statistics with Applications*. Cengage Learning.

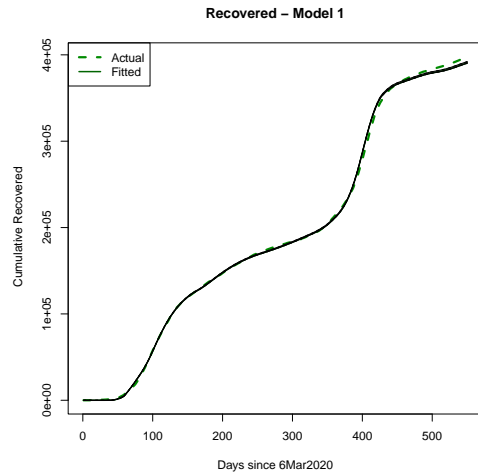
Willyard, C. (2023). Are repeat covid infections dangerous? what the science says. *Nature*, 616(7958):650–652.

Model	Parameter	Description	Mean Estimated Values	Quantiles (0.025 & 0.975)	Pseudo- R^2
Model 1	α_0	Transmission rate before intervention	0.00286	(0.00246, 0.00306)	0.99176
	α_1	Transmission rate after the first intervention	0.00084	(0.00081, 0.00087)	
	α_2	Transmission rate after the second intervention	0.00091	(0.00089, 0.00095)	
	α_3	Transmission rate after the third intervention	0.00076	(0.00075, 0.00077)	
	α_4	Transmission rate after the fourth intervention	0.00110	(0.00109, 0.00111)	
	α_5	Transmission rate after the fifth intervention	0.00089	(0.00088, 0.00090)	
	α_6	Transmission rate after the sixth intervention	0.00086	(0.00085, 0.00088)	
	α_7	Transmission rate after the seventh intervention	0.00097	(0.00097, 0.00099)	
	α_8	Transmission rate after the eighth intervention	0.00112	(0.00112, 0.00113)	
	α_9	Transmission rate after the ninth intervention	0.00132	(0.00246, 0.00306)	
	β	Rate at which the exposed becomes infectious (Infectious rate)	0.06988	(0.06939, 0.07075)	
	γ_{10}	Recovery rate from infections influenced by intervention	0.09097	(0.05473, 0.10933)	
	γ_{11}	Recovery rate from infections influenced by intervention	0.13564	(0.13499, 0.13883)	
	γ_{12}	Recovery rate from infections influenced by intervention	0.14758	(0.14192, 0.14847)	
	γ_{13}	Recovery rate from infections influenced by intervention	0.11333	(0.11300, 0.11370)	
	ϕ_1	Reinfection rate influenced by intervention	0.00538	(0.00528, 0.00543)	
	ϕ_2	Reinfection rate influenced by intervention	0.01187	(0.01170, 0.01244)	
	ϕ_3	Reinfection rate influenced by intervention	0.02213	(0.02118, 0.02312)	
	ϕ_4	Reinfection rate influenced by intervention	0.00740	(0.00679, 0.00805)	
	γ_2	Recovery rate from Reinfections	0.14295	(0.14295, 0.14295)	
μ	Vaccination rates	0.00460	(0.00000, 0.00920)		
κ	Vaccine efficacy	0.94	(0.94, 0.94)		
η	Deaths rate	0.00021	(0.00021, 0.00021)		
ζ_1	Natural immunity waning rate	0.00202	(0.00001, 0.00046)		
ζ_2	Immunity due to vaccination waning rate	0.00119	(0.000170, 0.00929)		
Model 2	α_0	Transmission rate before intervention	0.00314	(0.00289, 0.00329)	0.99160
	α_1	Transmission rate after the first intervention	0.00089	(0.00084, 0.00093)	
	α_2	Transmission rate after the second intervention	0.00089	(0.00089, 0.00090)	
	α_3	Transmission rate after the third intervention	0.00077	(0.00076, 0.00079)	
	α_4	Transmission rate after the fourth intervention	0.00110,	(0.00109, 0.00110)	
	α_5	Transmission rate after the fifth intervention	0.00090	(0.00088, 0.00091)	
	α_6	Transmission rate after the sixth intervention	0.00087	(0.00086, 0.00088)	
	α_7	Transmission rate after the seventh intervention	0.00098	(0.00097, 0.00099)	
	α_8	Transmission rate after the eighth intervention	00114	(0.00113, 0.00115)	
	α_9	Transmission rate after the ninth intervention	0.00135	(0.00289, 0.00329)	
	β	Infectious rate	0.07270	(0.06963, 0.07616)	
	γ_{10}	Recovery rate from infections influenced by intervention	0.11527	(0.09406, 0.12748)	
	γ_{11}	Recovery rate from infections influenced by intervention	0.13595	(0.13537, 0.13651)	
	γ_{12}	Recovery rate from infections influenced by intervention	0.15138	(0.14984, 0.15178)	
	γ_{13}	Recovery rate from infections influenced by intervention	0.11501	(0.11460, 0.11544)	
	ϕ_1	Reinfection rate influenced by intervention	0.01885	(0.01829, 0.01945)	
	ϕ_2	Reinfection rate influenced by intervention	0.01978	(0.01902, 0.02071)	
	ϕ_3	Reinfection rate influenced by intervention	0.02315	(0.02159, 0.02480)	
	ϕ_4	Reinfection rate influenced by intervention	0.01149	(0.01041, 0.01260)	
	γ_2	Recovery rate from Reinfections	0.14286	(0.14286, 0.14286)	
μ	Vaccination rates	0.00462	(0.0000, 0.00925)		
κ	Vaccine efficacy	0.94	(0.94, 0.94)		
η	Deaths rate	0.00021	(0.00021, 0.00021)		
ζ_1	Natural immunity waning rate	0.05374	(0.00090, 0.10646)		
ζ_2	Immunity due to vaccination waning rate	0.00359	(0.00000, 0.00229)		

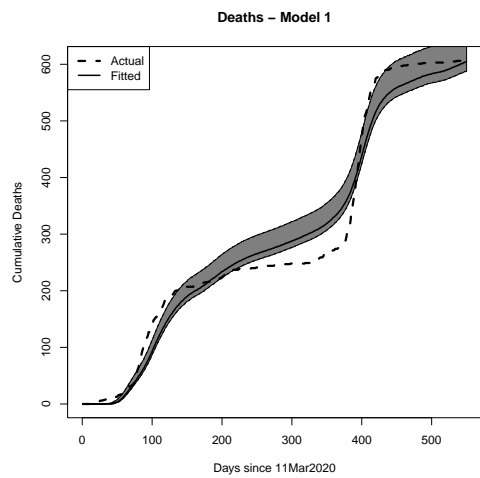
Table 2: Estimated $S_1EIRDVS_2IIR_R$ (Model 1) and SEIRDVIIR_R (Model 2) model parameters. These parameter values are estimated using the 50,000 posterior samples. Times are in days, rates are individuals per day, except α , ζ_1 and ζ_2 with rates in 10,000 individuals per day .



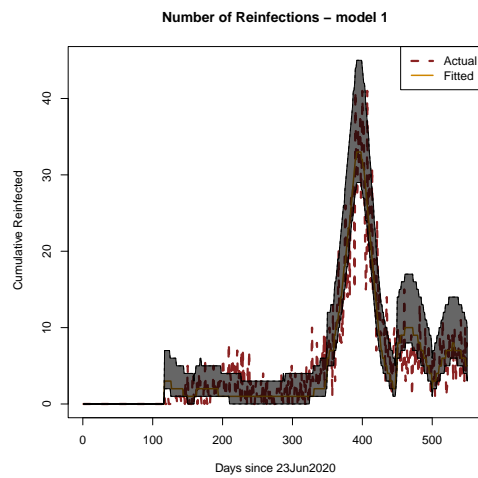
(a)



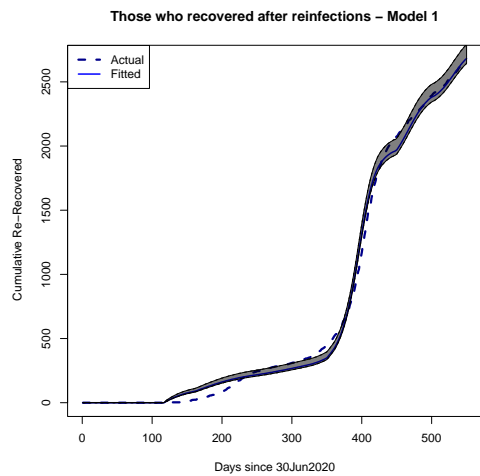
(b)



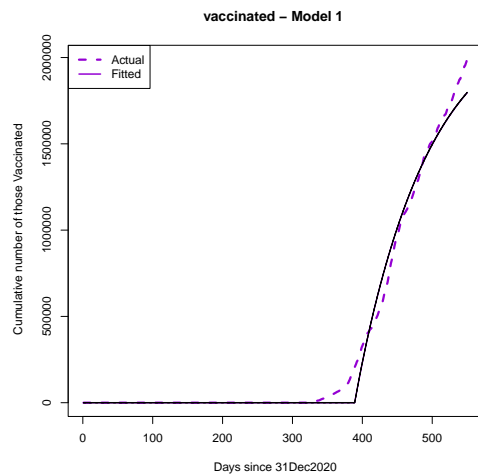
(c)



(d)

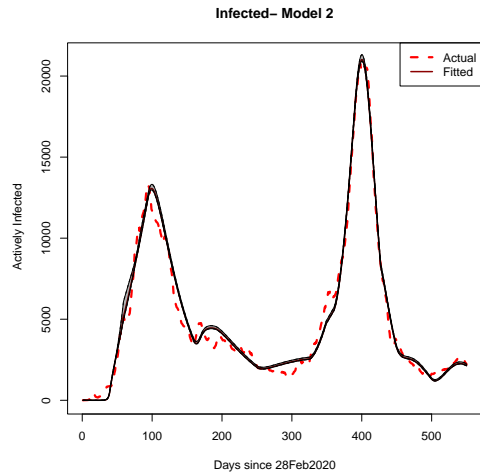


(e)

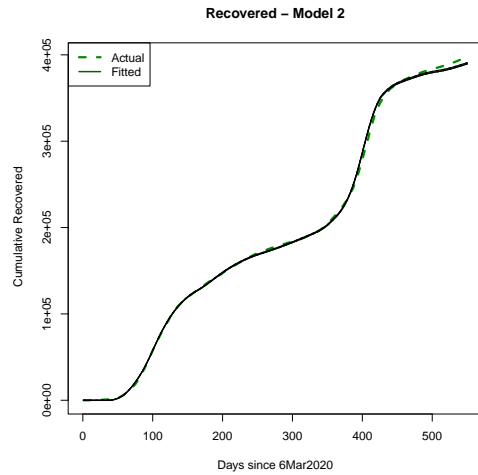


(f)

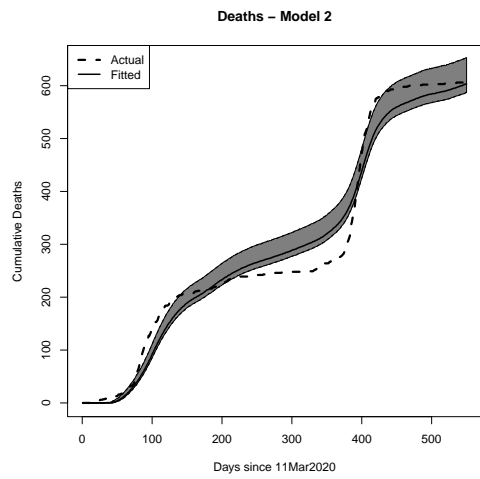
Figure 3: Plots of (a) Active Infections, (b) Cumulative Recovered, (c) Cumulative Deaths, (d) Number of Reinfections, (e) Cumulative Recovered after reinfections and (f) Cumulative number of Vaccinated for Model 1. The estimated quantiles (0.025, 0.5, and 0.975) were calculated using 50,000 samples from the posterior distribution.



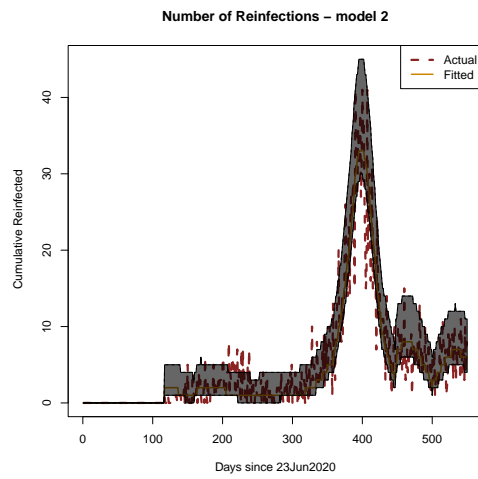
(a)



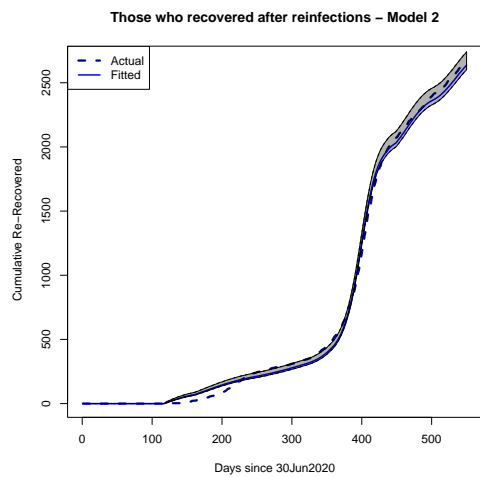
(b)



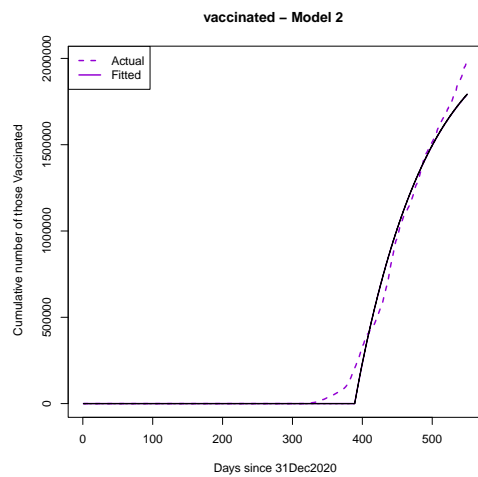
(c)



(d)

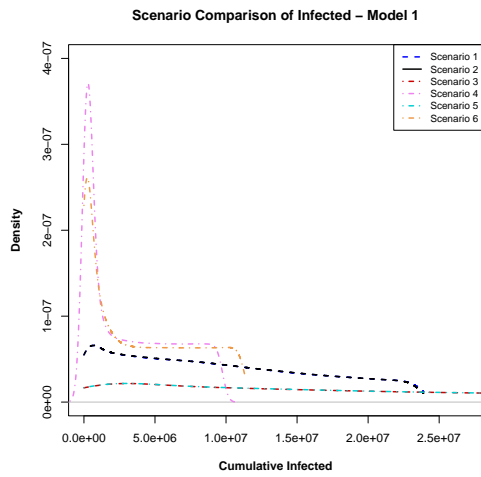


(e)

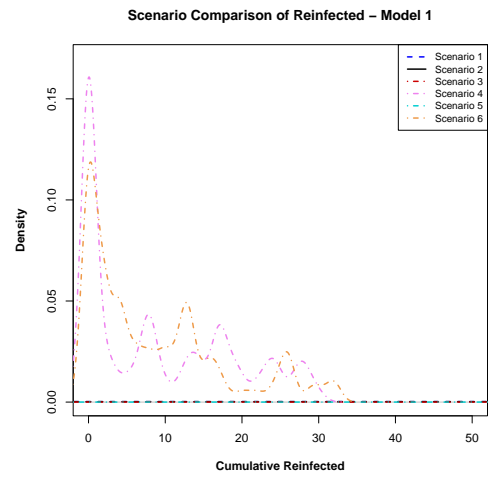


(f)

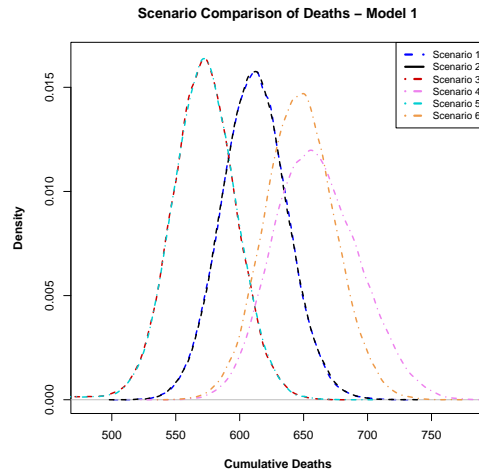
Figure 4: Plots of (a) Active Infections, (b) Cumulative Recovered, (c) Cumulative Deaths, (d) Number of Reinfections, (e) Cumulative Recovered after reinfections and (f) Cumulative number of Vaccinated for Model 2. The estimated quantiles (0.025, 0.5, and 0.975) were calculated using 50,000 samples from the posterior distribution.



(a) Comparison of PPDs for Cumulative Infected

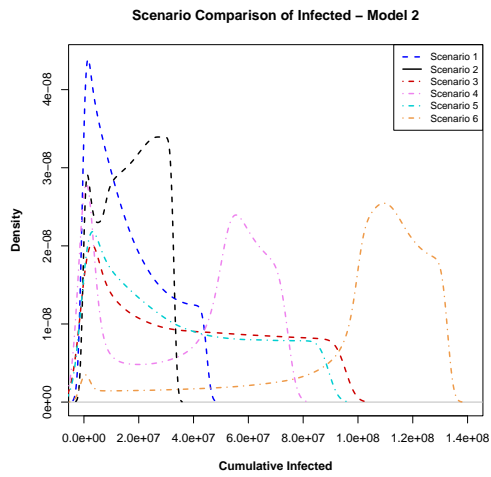


(b) Comparison of PPDs for Cumulative Reinfected

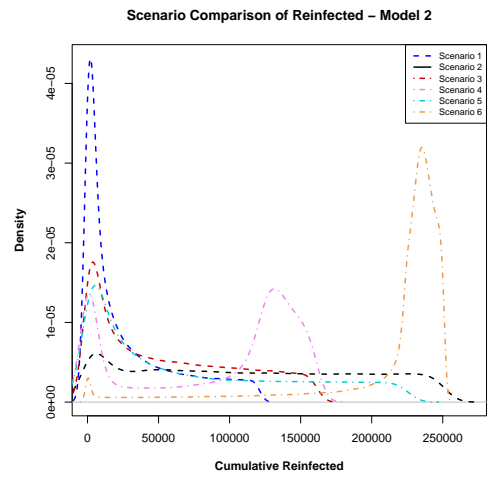


(c) Comparison of PPDs for Cumulative Deaths

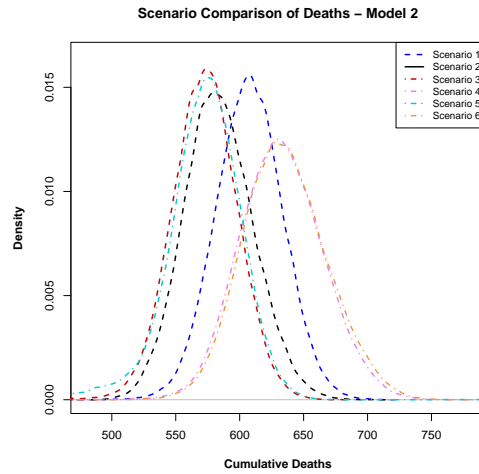
Figure 5: Plots of posterior predictive distributions (PPD) of (a) cumulative Infected, (b) Cumulative Reinfected and (c) Cumulative Deaths at day 540, obtained from Model 1. These were obtained using 50,000 samples from the posterior predictive distribution.



(a) Comparison of PPDs for Cumulative Infected



(b) Comparison of PPDs for Cumulative Reinfected



(c) Comparison of PPDs for Cumulative Deaths

Figure 6: Plots of posterior predictive distributions (PPDs) of (a) cumulative Infected, (b) cumulative Reinfected and (c) cumulative Deaths at day 540, obtained from Model 2. This was obtained using 50,000 samples from the posterior predictive distribution.